Subtidal flow division at a shallow tidal junction

F. A. Buschman,[1] A. J. F. Hoitink,[1,2] M. van der Vegt,[1] and P. Hoekstra[1]

Received 5 March 2010; revised 10 September 2010; accepted 20 September 2010; published 3 December 2010.

[1] Tides influence distribution of river discharge at tidally affected channel junctions. At the apex of a channel network in an Indonesian delta, observations of flow division suggest that tidally averaged flow division depends on the tidal range. To understand the mechanisms governing the subtidal flow division, an idealized hydrodynamic junction model inspired by the observations has been set up. The barotropic model consists of two exponentially converging tidal channels that connect to a tidal river at the junction and solves the nonlinear shallow water equations. By varying the depth, length, *e*-folding length scale of the channel width, and hydraulic roughness in one of the two tidal channels, the sensitivity of the subtidal flow division to those four parameters was investigated. For depth, length, and *e*-folding length scale differences between channels the effect of tides is generally to enhance unequal subtidal flow division that occurs in the case of river flow only. In contrast, for hydraulic roughness differences, the tidal effect partly cancels the inequality in river flow division. The tidal effect may even reverse the horizontal flow circulation that would occur in the absence of tides.

Citation: Buschman, F. A., A. J. F. Hoitink, M. van der Vegt, and P. Hoekstra (2010), Subtidal flow division at a shallow tidal junction, *Water Resour. Res.*, *46*, W12515, doi:10.1029/2010WR009266.

1. Introduction

[2] The processes governing the division of water at river bifurcations have received ample attention in the literature. When the geometry of the river junction and the upstream channel are symmetric about the line through the center of the upstream channel, the division of water over the two downstream channels is controlled by the channel dimensions and the hydraulic roughness in the two downstream channels [e.g., *Wang et al.*, 1995]. Asymmetries upstream of the river junction may also affect the flow division [*Bolla Pittaluga et al.*, 2003]. Examples of such asymmetries include different channel directions with respect to the feeding river channel [*Ramamurthy et al.*, 2007] and a bend upstream of the junction [*Kleinhans et al.*, 2008]. Due to these upstream asymmetries, the water surface slope close to the river junction may be larger in one of the two downstream channels [*Edmonds and Slingerland*, 2008; *Kleinhans et al.*, 2008], resulting in a larger share of river discharge into that channel.

[3] In comparison with river junctions, flow division at tidal junctions is complicated by tides that intrude from the mouths of the tidal channels. This paper focuses on the tidally averaged (hereinafter referred to as subtidal) flow division at tidal junctions characterized by a tidal velocity amplitude of 1–10 times the river flow velocity at the tidal junction. Recent observations of flow division at a tidal junction in Indonesia with depths around 5 m suggest that subtidal flow division changes with tidal range (section 2). The primary aim of this paper is to investigate the sensitivity of subtidal flow division to depth, length, bed roughness and river discharge. Understanding the subtidal flow division at shallow tidal junctions is important, since it may control the pathways of terrestrial sediments, nutrients and contaminants in tidal channel networks.

[4] A tidal wave that propagates into a natural shallow channel may paradoxically exhibit properties of both progressive and standing waves [*Friedrichs and Aubrey*, 1994]. Like for a progressive wave, in strongly convergent friction dominated channels the barotropic tidal wave propagates with a phase speed of approximately $\sqrt{gh}$, where g denotes the gravitational acceleration and h is the still water depth (see also the notation section). If the effects of friction balance effects of width convergence (i.e., funneling), the tidal range remains similar along the channel. Like a classical standing wave, the phase of flow velocity with respect to water surface level tends to 90 degrees in strongly convergent channels [*Jay*, 1991; *Friedrichs and Aubrey*, 1994].

[5] As the tide propagates landward in a shallow channel, the tidal waveshape is distorted by the generation of superharmonics [*Friedrichs and Aubrey*, 1988; *Parker*, 1991]. Usually, flood flows tend to become more intense and shorter and ebb flows tend to become longer and weaker. This generation of tidal asymmetry can be intensified by river discharge, because it amplifies friction, which is a principal cause of the distortion of tides [*Godin*, 1991; *Kukulka and Jay*, 2003].

[6] When water surface level and flow velocity covary, a landward transport of water occurs. This Stokes flux is maximal when water surface level and flow velocity are in phase, and is absent when the phase difference is 90 degrees. In a single channel the Stokes flux is compensated by a seaward directed Eulerian mean flux, generated by a subtidal

[1]Institute for Marine and Atmospheric Research Utrecht, Department of Physical Geography, Faculty of Geosciences, Utrecht University, TC Utrecht, Netherlands.
[2]Hydrology and Quantitative Water Management Group, Department of Environmental Sciences, Wageningen University, Wageningen, Netherlands.

0043-1397/10/2010WR009266

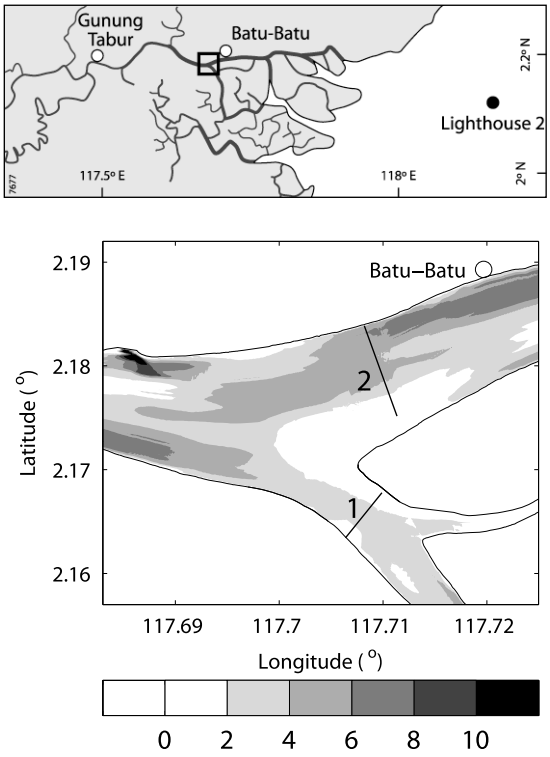

Figure 1. (top) Topographical map of the Berau region, showing the location of the apex junction (box) close to Batu-Batu and the rest of the Berau tidal channel network. (bottom) Bathymetry in the box, showing depths (m) below mean sea level and the navigated cross transects to obtain discharge estimates in channels 1 and 2.

pressure gradient. When tidal channels join, the tidal waves that propagate landward in the channels affect each other. In each of the three channels connected to the junction, tidal energy can propagate in two directions. The physical system is constrained by one water surface level at the tidal junction. Flow velocity amplitudes and phases in the three tidal channels, however, are not necessarily the same. Therefore, in a channel network the Stokes flux and return flow in general do not balance in each individual channel and net discharge may be generated in the downstream channels.

[7] The river discharge acts to redistribute and dissipate tidal energy, due to the strong effect of a net flow on friction [*Godin and Martínez*, 1994; *Horrevoets et al.*, 2004]. The effects of river-tide interaction on flow in a single tidal channel are most pronounced in parts of the channel where river flow velocity is substantial with respect to the tidal flow velocity amplitude. *Buschman et al.* [2009] provided an analysis revealing that subtidal friction can be decomposed into contributions due to (1) river discharge, (2) river-tide interaction and (3) tidal asymmetry inherent to the sum of tidal harmonics. Subtidal friction, in turn, is balanced by the pressure gradient due to the subtidal gradient water level setup. *Buschman et al.* [2009] used their analysis of the subtidal momentum balance to explain subtidal water level dynamics.

[8] Existing modeling studies addressing tidal network junctions are rare. *Hill and Souza* [2006] show that the mass and momentum equations may be linearized for a network of deep channels. They applied their analytical model successfully to a fjordic region. *Fagherazzi et al.* [2008] proposed an analytical method to link the morphologic characteristics of a creek channel to flow properties. Their method was designed to model salt marsh hydrodynamics, and falls short when the propagation of the tide within the channel network is not instantaneous. *Ridderinkhof* [1988] and *Buijsman and Ridderinkhof* [2007] show that subtidal flows in the shallow Wadden Sea, which is enclosed between barrier islands and the coast of the Netherlands, occur from the inlet channels that have a large tidal range to inlets with lower tidal range. These subtidal flows reflect the effect of nonlinearities in the shallow water equations, which were the basis of the model by *Ridderinkhof* [1988]. Residual flows in tidal channel networks were also considered by *Warner et al.* [2003]. In a channel network that is tidally driven from entrances on opposite sides, they showed that the residual flows are controlled by the temporal phasing and spatial asymmetry of the two forcing tides. In the present contribution we study the effect of tides on subtidal flow division at a junction and show that even for equal tidal forcing in a tidal network, residual flows can develop as a result of asymmetries in depth, length, width convergence or bed roughness between the different seaward channels that connect to the junction.

[9] This paper continues with a description of the field site and the results of discharge measurements in section 2. Section 3 describes an idealized barotropic model of flow division at a shallow tidal junction, which will be used to gain a basic insight in the mechanisms governing subtidal flows at shallow junctions in the parameter range of the Berau network. The idealized model consists of three channels interconnected at a junction, imposing the same tidal boundary conditions at two of the channels and a river discharge at the remaining channel. In section 4 the response of subtidal flow divisions at the idealized junction model to asymmetries in depth, length, width convergence and bed roughness are analyzed. The sensitivity to river discharge is analyzed for the case of a depth asymmetry. The implications of the results and a summary of the primary findings are described in the sections 5 and 6. The used symbols are listed in the notation section, which can be found after section 6.

2. Motivation: The Berau Channel Network

[10] Flow division was observed at the delta apex junction of the Berau system, located along the east coast of Kalimantan, Indonesia (Figure 1). The river discharge during these observations was about 500 $m^3\ s^{-1}$ [*Buschman et al.*, 2009], implying an average subtidal flow velocity of about 0.1 $m\ s^{-1}$ at the two cross sections of the tidal junction (Figure 1, bottom). Tides propagate into the Berau tidal channel network at three neighboring channel mouth regions. Tidal range at Lighthouse 2 station is around 1 m at neap tide and about 2.5 m at spring tide, and features a pronounced diurnal inequality. From the three west-east oriented branches, the northern channel is shallowest with a typical mean depth of 5 m, the middle channel is about 7 m deep and the southern channel is deepest having a mean depth of 10 m. For these three channels and the tidal river up to the village of Gunung Tabur, the tidal range remains similar.

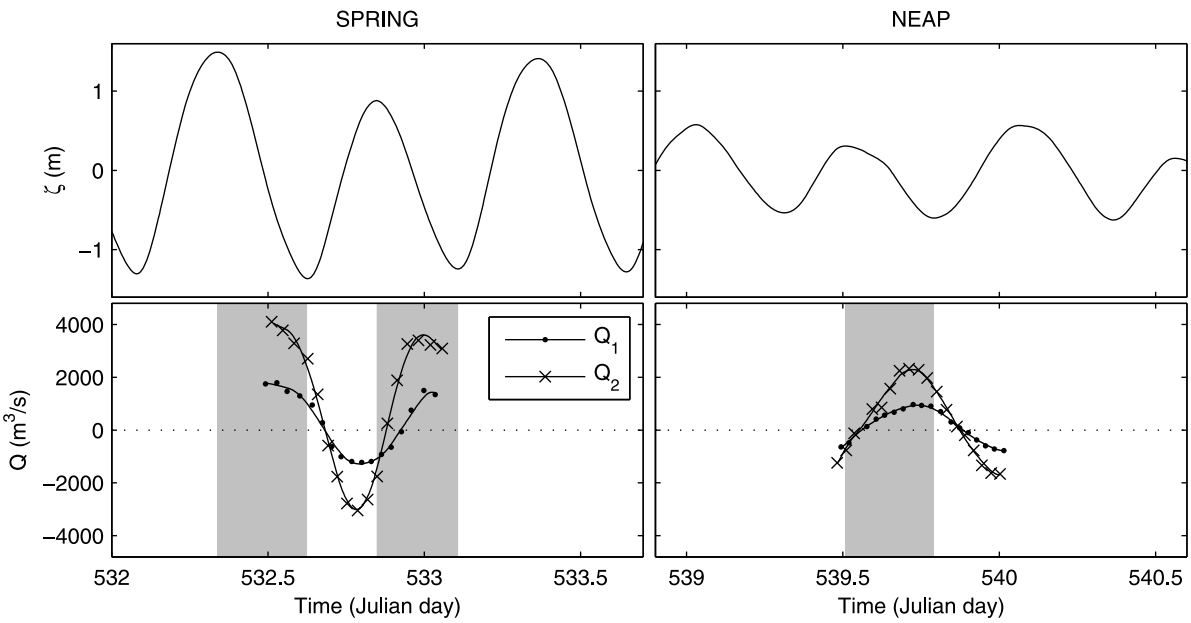

Figure 2. (top) Measured water surface level at Batu-Batu and (bottom) discharges obtained in channels 1 and 2 for a spring and a neap tidal period. Positive discharge corresponds to a seaward flow direction, and shaded periods denote falling tide.

[11] Discharge was observed by sailing transects along the two cross sections indicated in Figure 1 (bottom) with a 1.2 MHz broadband RD Instruments acoustic Doppler current profiler (ADCP). From the measured velocity profiles discharge was calculated using the methods of *Muste et al.* [2004], who estimate the error in the obtained discharge at 2.5% of the obtained value. The velocity measurements were projected on a grid at the two sections across the channels and along-channel velocity profiles were extrapolated to the bed and water surface, adopting a power law profile. The discharges through the sections near the banks without flow measurements were obtained from one third of the depth mean velocity measured closest to the bank and the cross sectional area determined from the bathymetry [*Boiten*, 2000]. The bathymetry was obtained from sailing transects across the channels about every kilometer with an echosounder and a GPS (Figure 1, bottom). For each sailed transect, discharge was obtained by integrating velocities over the cross section.

[12] The obtained discharge series in channels 1 and 2 near the apex junction covered 12.5 h during spring tide and during the subsequent neap tide. Figure 2 shows the discharges, which are smoothed using a quadratic LOESS filter with a turnover period of 4 h [*Schlax and Chelton*, 1992], and the water surface level variation that was observed close to the tidal junction in channel 2, at Batu-Batu village. Although the discharge observation period of 12.5 h is insufficient to completely separate the residual discharge from the diurnal tidal motion, the observations suggest that subtidal flow division depends on tidal range.

[13] Figure 2 shows that peak discharges during ebb and flood are around 2.3 times higher in channel 2, whereas the cross-sectional area is 2.8 times higher than in channel 1. We hypothesize that the higher peak flow velocities in channel 1 are related to the relatively small depths in the northern branch, as compared to the depths in the middle and southern branches that influence the flow in channel 2. As higher flow velocity amplitudes increase subtidal friction, this would imply that river flow velocities into channel 1 are smaller than into channel 2. If this hypothesis is valid, this effect should be most pronounced at spring tide when largest differences in tidal range occur between the channels.

[14] Figure 2 shows another indication that the division of subtidal discharge cannot simply be predicted from the ratio of the wetted cross-sectional areas of the two channels. During spring tide high water (HW) slack occurs 1.1 h later in channel 1 than in channel 2, whereas the LW slack occurs nearly simultaneously. At neap tide, the HW and LW slacks occur nearly simultaneously in the two channels. This may imply that a larger share of the river discharge is conveyed by channel 2 during spring tide than during neap tide. These results motivated the modeling study in sections 3 and 4, which aims to better understand the division of river discharge at shallow tidal junctions.

3. Barotropic Modeling of Flow Division

3.1. Model Setup

[15] A flow model was built using the Delft3D modeling environment. The depth-averaged (2DH) version was used, which solves the unsteady shallow water equations as described by *Lesser et al.* [2004]. The 2DH model was preferred over a one-dimensional alternative, because cross-channel flow at the tidal junction may occur when flow is from one channel at the sea side of the junction to the other. Moreover, flow division can be a function of the angle between the two channels on the sea side of the junction [*Edmonds and Slingerland*, 2008; *Ramamurthy et al.*, 2007]. The depth averaged version of Delft3D was selected instead of the 3D version, since 3D flow patterns are unimportant for the subtidal flow division in the idealized model. The occurring bend curvature is small, we neglect the effect of vertical and horizontal density differences, and if depth variations are present, they are gradual. Furthermore,

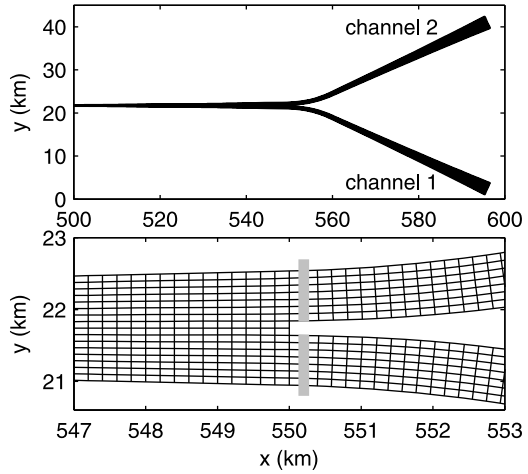

Figure 3. (top) The seaward part of the model grid, including a river part and two channels that connect the sea, which is on the right. (bottom) The grid in the surroundings of the tidal junction and the cross sections where discharges are stored from the model results (grey lines).

Lesser et al. [2004] showed that for several coastal examples results of 2DH simulations and 3D simulations were similar.

[16] The model grid is based on the apex junction at Batu-Batu (Figure 3). The grid was built with a grid generation programme that was previously used to build river junction grids for Delft3D [*Kleinhans et al.*, 2008]. In the default setting, the tidal junction is situated 50 km from the open sea boundary (Figure 3, top), analogous to the distance from the tidal junction close to Batu-Batu to the 10 m isobath in the nearshore zone. The river in the model is 550 km long to ensure that tides propagating up the river damp out smoothly. In the upstream 500 km of the river the width (W_{up}) is set at 357 m. At 500 km from the upstream boundary of the river section, the width of the channel (W) increases exponentially, according to

$$W = W_{up} e^{s/L_W}, \quad (1)$$

where L_W is the e-folding length for width and s is the along-channel coordinate, defined positive seaward. Analogously to the Berau case, the default setting of L_W was 33.3 km. This results in a width at the tidal junction of 1.60 km.

[17] In the whole model domain the grid cell length along the center line of the three channels was fixed at 200 m. For the channel landward of the junction the total channel width was equally divided over 16 grid cells across the channel. At the tidal junction, this channel splits into channels 1 and 2 (Figure 3, bottom). To split a channel, two rows of cells have to disappear seaward of the junction for numerical reasons [*Kleinhans et al.*, 2008]. Channels 1 and 2 were both 7 grid cells wide. By applying these grid characteristics, only 1/8th of the cross-sectional area was lost due the disappearing cells seaward of the junction. The ratio of length and width of a grid cell was 2 at the tidal junction and increases gradually going landward. The relatively small ratio at the junction can account for the substantial cross-channel flows that can occur immediately landward of the junction. The grid was nearly orthogonal everywhere.

Table 1. Default Parameter Setting in Idealized Junction Model

Symbol	Variable	Default Value
Δx	along-channel grid size	200 m
Δy	cross-channel grid size	22–450 m
Δt	time step	30 s
h	still water depth	5 m
L	length of seaward channel	50 km
L_W	e-folding length for width	33.3 km
W_{up}	width of upstream river	357 m
C	Chézy coefficient	55 $m^{1/2}$ s^{-1}
A_h	horizontal eddy viscosity	10 m^2 s^{-1}
$\langle Q \rangle$	river discharge	500 m^3 s^{-1}
a_{M2}	M_2 amplitude at sea	0.7 m
a_{S2}	S_2 amplitude at sea	0.4 m

[18] A time step of 30 s was used in all calculations. Grid sensitivity tests showed that increasing the time resolution did not significantly alter the results. Doubling the temporal and spatial resolution resulted in only 1.5% changes in tidal and subtidal velocities.

[19] The default value for hydraulic roughness, expressed as a Chézy coefficient, was 55 $m^{1/2}$ s^{-1}, which is a common hydraulic roughness value for tidal channels. The horizontal eddy viscosity was set to 10 m^2 s^{-1}. In the default setting, the model is forced with a river discharge of 500 m^3 s^{-1} at the upstream boundary. At the sea boundaries the model was forced with a M_2 tidal harmonic with an amplitude of 0.7 m and a S_2 tidal harmonic with an amplitude of 0.4 m, resulting in a spring-neap cycle. To ensure that the equilibrium depth was 5 m in the upper river channel, the bottom slope was fixed at -5.2×10^{-6}. The rest of the model domain features a horizontal bottom. The model runs covered 23 days for each simulation, including a spring-neap period of 14.7 days and spin-up time. The initial conditions of all model simulation consisted of zero flow velocity and an initial water depth of 5 m in the entire modeling domain. An overview of all default parameter settings is given in Table 1.

3.2. Setup of the Sensitivity Analysis

[20] Four series of simulations were carried out in which only one parameter in channel 1 was changed (Table 2), with the other parameters fixed at their default setting (Table 1). The still water depth and hydraulic roughness were varied with respect to the default value in the 45 km on the sea side of channel 1. From the junction to 5 km into channel 1 depth and hydraulic roughness gradually merged with the default settings, based on linear interpolation. This ensured that no strong flow irregularities arose in the model. In the third and fourth series of simulations, the channel length and the e-folding length scale for width were systematically varied

Table 2. Series of Simulations Performed With the Idealized Junction Model

Variable	Channel 1
h	3–10 m
L	10–100 km
L_W	13.3–53.3 km
C	25–105 $m^{1/2}$ s^{-1}
$\langle Q \rangle$	100–1500 m^3 s^{-1} and h_1 =10 m

Table 3. Different Forcing Conditions Applied to the Tidal Junction Model

Subscript	River Discharge ($m^3\ s^{-1}$)	Tidal Amplitude (m)
rt (default)	500	$a_{M2} = 0.7$, $a_{S2} = 0.4$
r	500	$a_{M2} = 0$, $a_{S2} = 0$
t	0	$a_{M2} = 0.7$, $a_{S2} = 0.4$

over the entire channel 1. In a fifth series of simulations the river discharge was varied. In that series of simulations the still water depth in channel 1 is 10 m and other parameters have their default value.

[21] Each sensitivity experiment was run with three different forcing conditions. In the default model forcing, hereinafter referred to with subscript rt, the model is forced with both tides and a river discharge (Table 3). To isolate the effects of tides, river discharge and river-tide interaction, parallel model simulations were run imposing the tidal water level variation only (referred to with the subscript t), and the river discharge only (subscript r).

3.3. Discharge Calculation and Discharge Asymmetry Index

[22] Discharges at the junction channels were calculated from the model results at the cross sections one grid cell seaward of the tidal junction. The specific discharges were integrated over the 7 grid cells across the width to yield the discharge in a channel. The subtidal discharge was obtained by applying a standard Godin filter [*Emery and Thomson*, 2001]. Residual discharges during spring tide and neap tide were obtained by averaging the subtidal discharges over two lunar days at the corresponding phase in the spring-neap cycle. Residual discharges are also averaged over a whole MSf period, which is a spring-neap period due to the combination of the M_2 and S_2 constituents.

[23] Hereinafter, subtidal flow division is presented as the difference in subtidal discharge between channels 1 and 2 divided by their sum:

$$\Psi = \frac{\langle Q \rangle_1 - \langle Q \rangle_2}{\langle Q \rangle_1 + \langle Q \rangle_2}, \tag{2}$$

where $\langle\rangle$ represents a tidal average. The discharge asymmetry index (Ψ) is 1 when all subtidal discharge flows through channel 1 and −1 when channel 2 conveys all subtidal discharge, provided that the subtidal discharge in each channel is directed seaward (defined positive). For the simulations forced with both river discharge and tides (denoted with subscript *rt*) both $\langle Q \rangle_1$ and $\langle Q \rangle_2$ are positive in all simulations.

[24] To distinguish between effects of tides, river discharge and their interaction on subtidal discharge, subtidal discharges were decomposed using the method of *Stein and Alpert* [1993]. To separate contributions and their interaction for two factors, river discharge and tides, four simulations are required [*Stein and Alpert*, 1993]. The model is run for three forcing conditions: tides only, river discharge only and both. Noting that for neither tidal nor river discharge forcing the subtidal discharge is zero, the subtidal discharge forced by both river flow and tides ($\langle Q \rangle_{rt}$) can be decomposed as

$$\langle Q_{rt} \rangle = Q_r + \langle Q \rangle_t + \langle Q \rangle_i, \tag{3}$$

where Q_r denotes the contribution solely due to river flow, $\langle Q \rangle_t$ the contribution due to tides alone and $\langle Q \rangle_i$ due to river-tide interaction. Similarly, the discharge asymmetry index can be split up as

$$\Psi_{rt} = \Psi_r + \Psi_t + \Psi_i. \tag{4}$$

4. Simulation Results

4.1. Sensitivity to Channel Depth

[25] Figure 4 shows how subtidal flow division depends on differences in still water depth at the mouth of channels 1 and 2. The results are shown for a tidal cycle during neap tide, one during spring tide, and averaged over an entire MSf period. Figure 4 also shows Ψ for the case that river discharge divides according to the cross-sectional areas at the mouth of the two channels (denoted by "Area" in the legend). In comparison with this reference case, Ψ_{rt} averaged over the three periods are larger in magnitude, favoring subtidal discharge to the deeper channel. It also shows that the subtidal discharge division tends to become more unequal with increasing tidal range. Values of Ψ_{rt} averaged over neap tide are closest to the reference case, which means that the total subtidal discharge is more equally divided over channels 1 and 2 during neap tide than during spring tide.

[26] Figure 5 shows the different contributions to Ψ_{rt} as a function of mean depth at the mouth of channel 1 during neap tide and during spring tide. Results obtained by averaging over a spring-neap cycle are in between the results of neap and spring tide (Figure 4). Both for spring and neap tide, magnitudes of Ψ_r are largest, followed by Ψ_t and finally Ψ_i. The difference between Ψ_{rt} and Ψ_r is principally due to tides (Ψ_t), which means that for this junction configuration the effects of tides on subtidal flow division are more important than effects of river-tide interaction. In general, Ψ_t increases with tidal range and has the same sign as Ψ_r. In conclusion, for a depth asymmetry, tides enlarge the share of the river discharge allocated to the deeper channel.

[27] To understand the effect of tides on subtidal discharge division, the contribution from simulations forced with tides only ($\langle Q \rangle_t$) is split in two components. To do so, the cross-sectional averaged flow velocity is decomposed according to $U = \langle U \rangle + U'$, where the prime denotes the zero

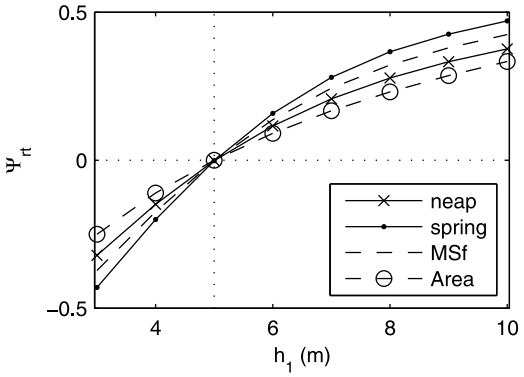

Figure 4. Sensitivity of the discharge asymmetry index to mean depth in channel 1 for different averaging periods and, as a reference case, to water distribution according to the cross-sectional area. The vertical dashed line denotes the mean depth in channel 2.

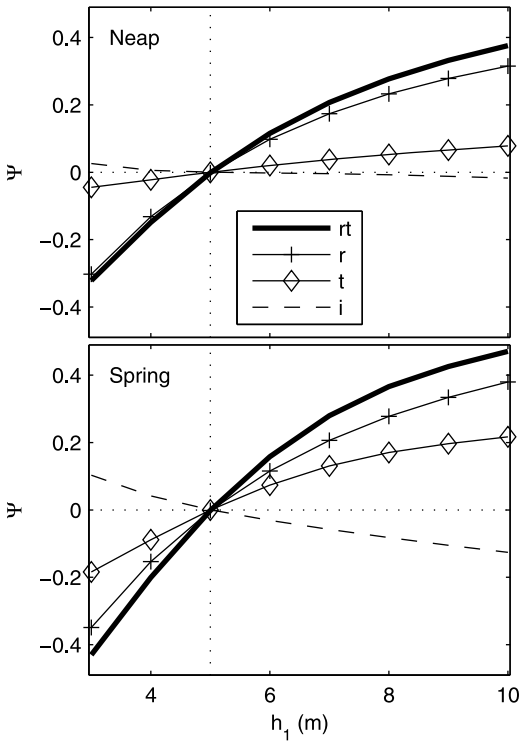

Figure 5. Decomposition of the discharge asymmetry index due to river and tidal forcing (Ψ_{rt}) into contributions from river discharge forcing only (Ψ_r), tidal forcing only (Ψ_t), and interaction of river and tides (Ψ_i).

mean variation during a tidal cycle. Similarly, depth can be written as $d = h + \langle\zeta\rangle + \zeta'$, where $\langle\zeta\rangle$ denotes the water surface level variation at the spring-neap period. Assuming a time-invariant channel width (W), subtidal discharge can be rewritten as

$$\langle Q\rangle_t = \underbrace{W\langle U'\zeta'\rangle}_{Q_s} + \underbrace{W(h+\langle\zeta\rangle)\langle U\rangle}_{Q_N}, \quad (5)$$

where Q_S denotes Stokes transport and Q_N denotes a return discharge. In general, Q_S is directed landward, generating a water level gradient that forces a net compensating return discharge seaward. The magnitudes of Q_N and Q_S can be highly nonuniform in convergent channels, being largest close to sea and decreasing going landward. However, in single tidal channels (having constant width or being convergent) the water storage is limited and Q_N and Q_S balance. Therefore $\langle Q\rangle_t$ is small or zero. In a channel of a network, Q_S and Q_N do not necessarily balance, implying that $\langle Q\rangle_t$ in the channels seaward of the tidal junction may have nonzero values.

[28] Figure 6 illustrates how tides induce a horizontal residual circulation from channel 1 into channel 2 when channel 2 is deeper. The distortion of the tidal wave in channel 1 is more pronounced due to larger friction. This results in a smaller tidal range and a larger phase difference between U and ζ (which both reduce the magnitude of Q_S) in channel 1 compared to channel 2. The sum of Q_{1S} and Q_{2S} must be compensated by a return discharge to sea. Due to the constraint of a single water surface level at the junction and at sea, the mean water level gradients from the junction to the sea are equal in the two channels. Due to larger relative importance of friction and the smaller cross-sectional area in channel 1, Q_{1N} is much smaller than Q_{2N}. Although the Stokes flux term has largest magnitude in the deeper channel 2, the net return flux is even larger. Thus, Q_{2N} exceeds $-Q_{2S}$, resulting in a seaward subtidal discharge in the deeper channel caused by the tides. The value of Q_{1N} is smaller than $-Q_{1S}$, yielding a negative $\langle Q\rangle_{1t}$ that has equal magnitude but opposing sign as $\langle Q\rangle_{2t}$. The results are qualitatively reversed for $h_1 > h_2$.

[29] The analysis above is not easily extended to the situation with a river discharge, since it is impossible to distinguish between Q_N and the river discharge. Interaction may occur that results in a dependence of Q_N on the river discharge. Also Q_S depends on river discharge, because river flow dampens the tides and influences the tidal propagation. For the simulations forced with both tides and river discharge, the effects of tides on $\langle Q\rangle_{rt}$ can be separated in the effect of tides only ($\langle Q\rangle_t$) and the effect of river-tide interaction ($\langle Q\rangle_i$) using the decomposition of equation (3).

[30] The sign of Ψ_i differs from the other two contributions (Figure 5), because river flow dampens the tidal flow velocities. Due to the dampening of the tidal flow in the simulation series with both river discharge and tidal forcing, Q_{1S} and Q_{2S} are smaller than in the series forced with only tides. The interaction of river and tidal flow reduces the tidal effect and thus opposes the effect of river flow only and tides only.

[31] To gain insight in the temporal variation of Ψ_{rt}, Figure 7 shows results of the simulations with $h_1 = 10$ m and $h_2 = 5$ m for an entire spring neap cycle. Total subtidal discharge peaks a day before neap tide and at spring tide it is lower than average. The principal reason is that at high tidal range the subtidal friction is relatively large, which leads to a larger subtidal water level gradient compared to neap tide [*Buschman et al.*, 2009]. Hence, water is temporarily stored in the network at spring tide. The smaller than average subtidal discharge before spring tide reflects this storing of water. Approaching neap tide, the total subtidal discharge is higher than the river discharge because the water is leaving the system again.

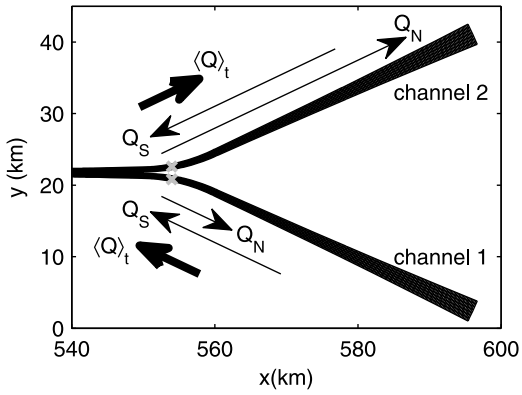

Figure 6. Schematic overview illustrating the decomposition of subtidal discharge by the tidal motion ($\langle Q\rangle_t$) into contributions of the Stokes transport (Q_S) and the net subtidal discharge (Q_N) at two cross sections seaward of a tidal junction (indicated by grey crosses) for the case that channel 1 is shallower than channel 2.

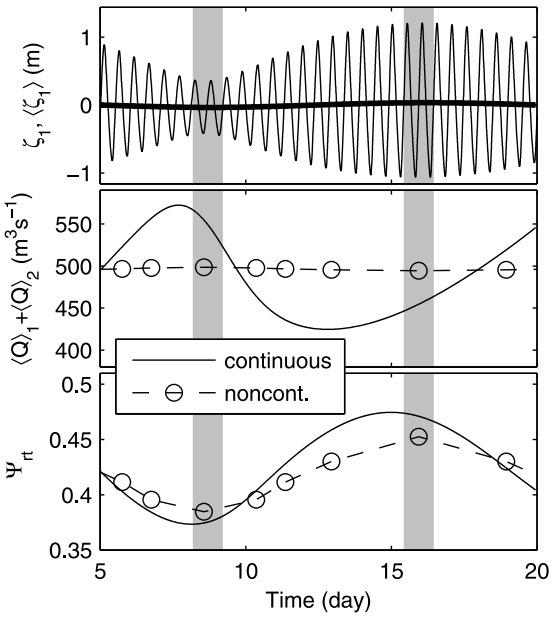

Figure 7. Temporal variation of the simulation results with largest subtidal depth in channel 1. The shaded areas denote the averaging periods at neap and spring tides. (top) The instantaneous and subtidal water surface level variation in channel 1 close to the junction. (middle) Total subtidal discharge from the simulation forced with M_2 and S_2 tides (continuous) and from a series of simulations forced with varying M_2 amplitude (noncontinuous). (bottom) Same for discharge asymmetry index.

[32] The fortnightly variation in the total subtidal discharge also affects the subtidal flow division. To distinguish between the effects induced by the fortnightly subtidal discharge variation and the effect of tidal range alone, simulations were performed with a_{S2} =0 m and stepwise changing a_{M2}. The results of this series of noncontinuous, steady state simulations are plotted in Figure 7 (middle and bottom). The differences in Ψ_{rt} obtained with the discrete simulations and with the continuous simulation forced with a_{M2} =0.7 m and a_{S2} = 0.4 m are not large. The continuous simulation has a larger variation in Ψ_{rt} over a spring-neap cycle and its extremes occur earlier. The MSf discharge enhances the inequality of the subtidal flow division due to tidal range solely, but the tidal effect on the discharge asymmetry index is primarily due to tidal range variation.

4.2. Sensitivity to Channel Length and Width

[33] Figure 8 shows the sensitivity of subtidal discharge division to the length of channel 1. Because width and depth variation are the same along channels 1 and 2, the longer channel has a wider channel mouth. When channel 1 is shorter than channel 2, the shorter distance from the junction to the channel mouth leads to a larger share of subtidal discharge. This effect is larger during spring than during neap tide. In contrast, when channel 1 is longer than channel 2, the discharge asymmetry index is nearly zero, implying an approximate equal subtidal discharge division.

[34] The results can be explained by looking at along-channel profiles of the mean water surface and tidal range (Figure 9). There is a clear concave mean water surface profile near the channel mouths. For L_1 = 20 km the region of influence of this effect extends to the junction, favoring discharge allocation to the shortest channel. For L_1 = 90 km, the concavity of the subtidal water level profile has largely faded before the tidal junction, causing mean surface level gradients in the immediate vicinity of the junction to be nearly equal in both channels (Figure 9, top right).

[35] Figure 10 shows contributions due to river flow only, due to tidal flow only and due to the interaction of river and tidal flow to Ψ_{rt} for spring tide conditions. When the length of channel 1 is smaller than 50 km, tides generally enhance the asymmetry in subtidal discharge division that occurs in the absence of tidal motion. The tidal effect on subtidal flow division is partly due to transfer of tidal energy from one channel seaward of the junction into the other. Because channel 1 is shorter, during parts of the tidal cycle a tidal energy flux enters channel 2 from channel 1, which results in relatively large tidal amplitudes in the near-junction part of the longer channel (Figure 9, bottom). The elevated flow velocity amplitudes in this part tend to increase subtidal friction, which increases with tidal flow velocity amplitude, residual current and their interaction [*Buschman et al.*, 2009]. In the subtidal momentum balance, subtidal friction primarily balances a subtidal water level gradient. The elevated subtidal friction in channel 2 implies a relative increase of subtidal discharge through the shorter channel 1, because only then does a balance between subtidal pressure gradient and friction occur in both channels. The subtidal discharge into the shorter channel 1 is thus enhanced by the higher tidal motion near the junction in channel 2.

[36] When the length of channel 1 is larger than 50 km tides favor subtidal discharge into the shorter channel 2, whereas for river forcing only no strong preference is modeled. In case of forcing the system with both tides and river discharge, the river-tide interaction balances the tide-induced unequal subtidal discharge division and the result is that discharge divides almost equally over the channels.

[37] Besides the effect of length differences, sensitivity of Ψ_{rt} to differences in width decay were analyzed. The results for spring tide (results not shown) are qualitatively the same as results for L_1 < 70 km (Figure 10). At the smallest *e*-folding length for width in channel 1 (strongest convergence of channel width), 13.3 km, the width at the channel mouth

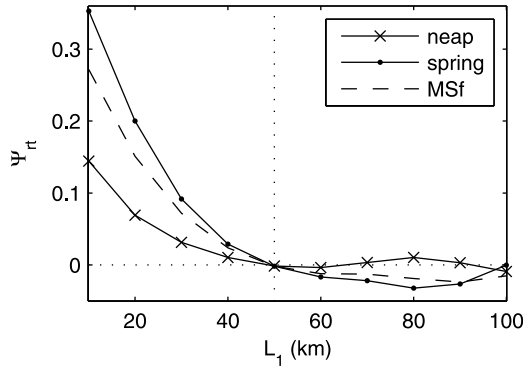

Figure 8. Discharge asymmetry index as a function of the channel length of channel 1 for different averaging periods. The vertical dashed line denotes the length of channel 2.

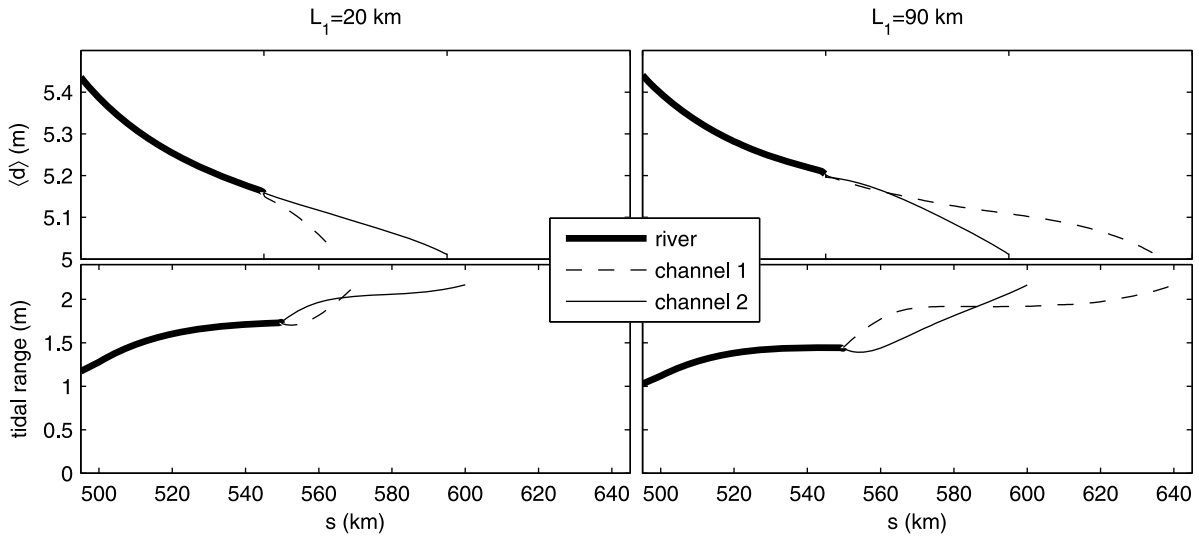

Figure 9. (top) Subtidal depth and (bottom) tidal range during spring tide as a function of the distance along the three channels for lengths in channel 1 of (left) 20 km and (right) 90 km.

was nearly 10 times larger in channel 1. Due to the larger mean cross sectional area, the river effect is to favor discharge into channel 1. The tidal effect enhances the river effect, but only marginally. When the *e*-folding length for width in channel 1 is larger than 13.3 km, the influence of tides on the discharge asymmetry index decreases further.

4.3. Sensitivity to Bed Roughness

[38] Figure 11 shows the response of Ψ_{rt} and the different contributions to differences in the square root of the bed friction coefficient ($\sqrt{c_{f1}}$), which equals $\sqrt{g}/C_1$. The discharge asymmetry index depends critically on the phase within the spring-neap cycle. For neap tide, the largest subtidal discharge occurs in the channel with the lowest bed roughness conditions. For spring tide conditions the largest subtidal discharge is in the channel with smallest hydraulic roughness when $\sqrt{c_{f1}} > 0.08$, but in the channel with largest hydraulic roughness for $\sqrt{c_{f1}} < 0.08$. Values of Ψ_{rt} averaged over an MSf period are in between the corresponding values pertaining to spring and neap tidal averages.

[39] Unlike the parameters studied so far, tides oppose the river effect for friction coefficient differences (Figure 12). Moreover, the effect of interaction of river and tidal flow does not necessarily oppose the tidal effect. The interaction and tidal effect may thus enhance each other, reducing the importance of the river effect.

[40] Focusing on neap tide conditions, the tidal motion exerts a negligible influence on Ψ_{rt}, which follows closely Ψ_r (Figure 12, top). For small bed friction coefficients in channel 1, the magnitude of Ψ_t approximates 10% of Ψ_r, yet is nearly completely canceled by Ψ_i. For high c_{f1}, Ψ_i has the same sign as Ψ_t, but their magnitudes are both small.

[41] Focusing on spring tide conditions, Ψ_t exceeds Ψ_r in absolute value for $\sqrt{c_{f1}} < 0.08$ (Figure 12, bottom). For this parameter range the Stokes flux (Q_S) is significantly larger in channel 1 than in channel 2, because tidal range and flow velocities are larger and the phase difference between U and ζ is smaller than in channel 2. At the same time, the return discharge in channel 1 (Q_{1N}) is only slightly higher than Q_{2N}. In case of hydraulic roughness differences between the two channels, tides force a subtidal discharge from the

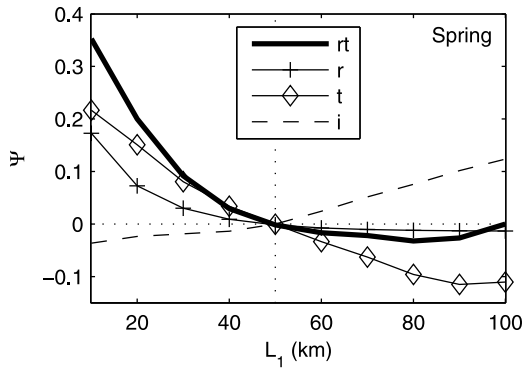

Figure 10. Decomposition of Ψ_{rt} as a function of L_1 into contributions from Ψ_r, Ψ_t and Ψ_i for spring tide.

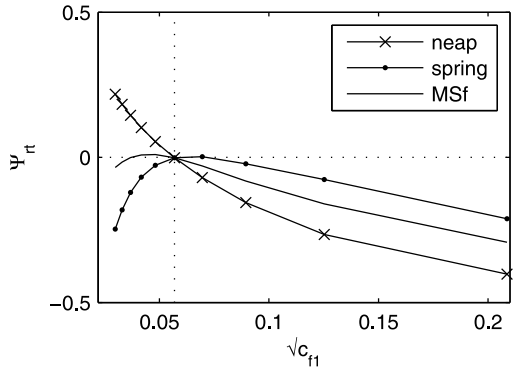

Figure 11. Discharge asymmetry index as a function of the square root of the bed friction coefficient in channel 1 for different averaging periods. The vertical dashed line denotes the simulation with the same bed roughness in channels 1 and 2.

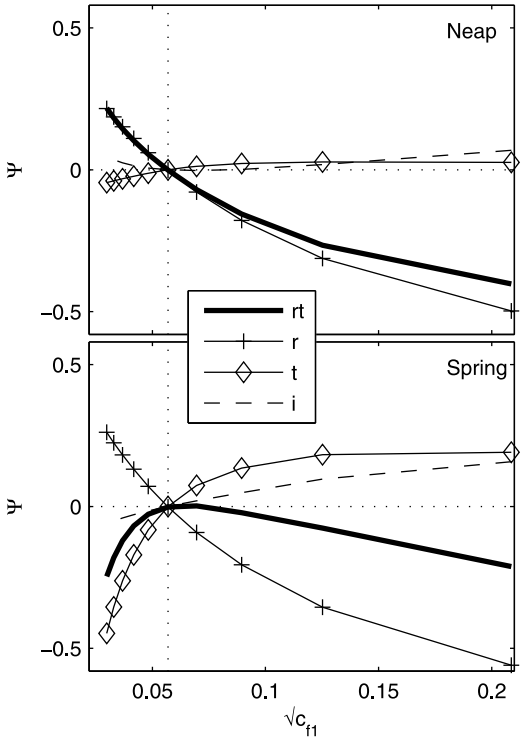

Figure 12. Decomposition of Ψ_{rt} as a function of the square root of the bed friction coefficient into contributions from Ψ_r, Ψ_t and Ψ_i for (top) neap tide and (bottom) spring tide.

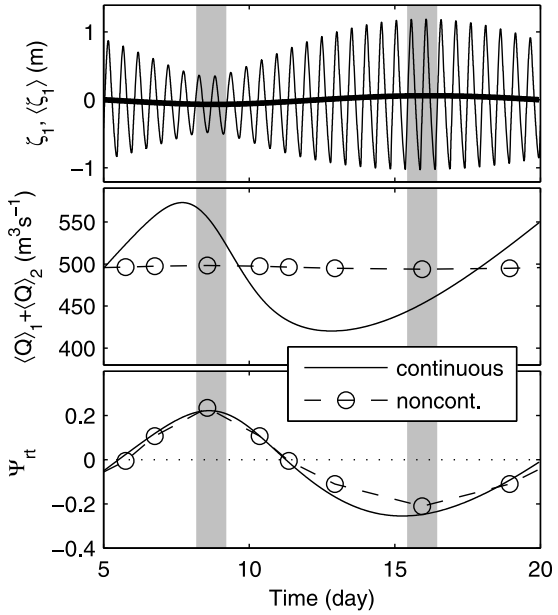

Figure 13. Temporal variation of the simulation results with $\sqrt{c_{f1}} = 0.030$. The shaded areas denote the averaging periods at neap and spring tide. (top) The instantaneous and subtidal water surface level variation in channel 1 close to the junction. (middle) Total subtidal discharge from the simulation forced with M_2 and S_2 tides (continuous) and from simulations forced with varying M_2 amplitude (noncontinuous). (bottom) Same for discharge asymmetry index.

channel with lower bed roughness to the channel with larger bed roughness. This opposes and in some cases even overwhelms the asymmetric discharge distribution induced by river flow.

[42] The discharge asymmetry induced by river-tide interactions (Ψ_i) enhances Ψ_t for all simulations during spring tide (Figure 12, bottom), whereas for depth and length differences Ψ_i and Ψ_t are opposing each other. Due to river-tide interactions both the Stokes flux (Q_S) and the return flux (Q_N) in channels 1 and 2 are smaller in magnitude than in the tides only simulation. Because the asymmetric distribution of subtidal discharge at the junction induced by the Stokes flux decreases less than that induced by the return flux, the total effect of river-tide interaction is to enhance the tide effect and oppose the river effect.

[43] To decompose the tidal effect on subtidal flow division (Ψ_{rt}) into the effect of tidal range solely and the effect of the fortnightly time lag for $\sqrt{c_{f1}} = 0.030$, we also calculated the discharge asymmetry indices from series of simulations forced with stepwise varying M_2 tidal amplitudes. Figure 13 (bottom) compares those noncontinuous, steady state results with the result of the simulation forced with both M_2 and S_2 tides. The effect of the fortnightly subtidal discharges on Ψ_{rt} is negligible in comparison with the tidal range effect, suggesting that for differences in bed friction coefficient tidal range determines Ψ_{rt} dominantly.

4.4. Sensitivity to River Discharge

[44] The sensitivity of the discharge asymmetry index to river discharge was investigated using the configuration with $h_1 = 10$ m and $h_2 = 5$ m. The bed slope in the river was kept constant, implying that water depths in the river are slightly higher at higher river discharges. Figure 14 shows that differences in Ψ_{rt} during spring tide and neap tide increase with decreasing river discharge. Since the discharge range at the junction for all simulations is 11 10^3 m^3 s^{-1} during spring tide and 4 10^3 m^3 s^{-1} during neap tide, it can be seen from Figure 14 that Ψ_{rt} varies nonlinearly with the ratio of river discharge and discharge range.

[45] The discharge asymmetry index is large when variation in discharge due to tides is large in comparison with the subtidal discharge. For the simulation with a river discharge

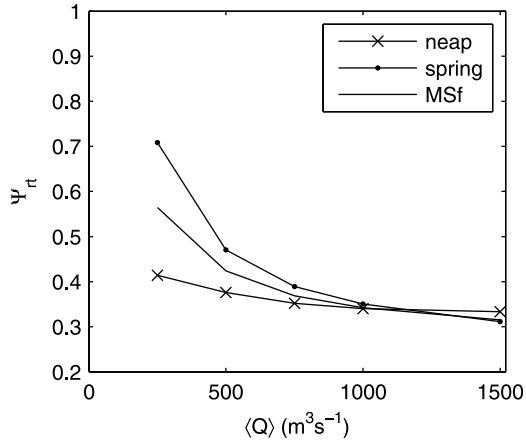

Figure 14. Sensitivity of the discharge asymmetry index to river discharge forcing for the configuration with $h_1 = 10$ m and different averaging periods.

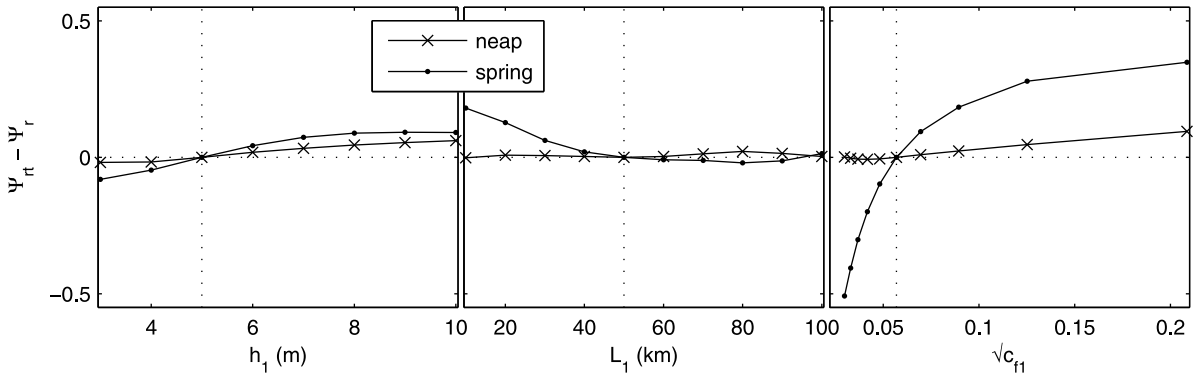

Figure 15. The effect of adding tides to a shallow junction system forced with river discharge only on the discharge asymmetry index as a function of (left) depth, (middle) channel length, and (right) the square root of the bed friction coefficient in channel 1. The vertical dashed lines denote the value of the variables in channel 2.

of 250 m^3 s^{-1}, for which river discharge is only 2% of the discharge range during spring tide, the tidal effect causes subtidal discharge to be primarily conveyed by the deeper channel 1. For river discharges higher than 750 m^3 s^{-1}, Ψ_{rt} is similar during spring and neap tide. This suggests that the tidal effect on discharge asymmetry is negligible when river discharge is larger than about 10 % of the semidiurnal discharge range.

5. Discussion

[46] Figure 15 summarizes the effect of tides on subtidal discharge distribution by showing $\Psi_{rt} - \Psi_r$ as a function of depth in channel 1, length of channel 1 and the square root of the bed friction coefficient in channel 1. Tidal motion generally favors the allocation of river discharge to deeper and shorter channels, enhancing the inequality in discharge distribution that would occur due to river flow. On the contrary, with differences in hydraulic roughness, tides counteract and sometimes overwhelm the unequal discharge distribution that occurs due to river discharge only. For the selected parameter regimes the magnitude of the tidal effect is largest for differences in hydraulic roughness. For the lowest bed friction coefficient in channel 1, spring tides reduce the subtidal discharge in channel 1 by a quarter of the total subtidal discharges in comparison with neap tide (Figure 15, right).

[47] The results of the idealized model forced with river discharge only show that depth differences have large effect on the discharge asymmetry index. The river discharge distribution is proportional to the ratio of the cross-sectional area at the mouth of the two channels, raised to the power 1.2 (Figures 4 and 5). This exponent is close to 1.25, which is the exponent found in studies on hydraulic geometry scaling relationships [*Edmonds and Slingerland*, 2007]. The tidal motion enhances the inequality in the discharge distribution, which can be captured in an increase of the exponent in the hydraulic geometry relation to 1.3 at neap tide and to 1.7 at spring tide (Figure 4).

[48] The sensitivity of the subtidal discharge distribution at the junction was studied for one parameter at a time. It should be noted that the joint effect of parameters is not simply the sum of the separate effects, due to the nonlinear behavior of the junction system. The merit of the present paper is to identify the underlying mechanisms that affect river discharge distribution under the influence of tides. These are the Stokes fluxes, the subtidal surface level gradients close to the tidal junction and tidal amplitudes, which control return currents by enhancing subtidal friction.

[49] To some extent, these quantitative results depend on the choices made in the setup and forcing of the model. The model was built in Delft3D using a finite difference scheme. Junction boundaries may be better represented with a finite element model that uses triangular cells [e.g., *Hanert et al.* 2005], which allow increases in the resolution locally near the junction. Such improvements are expected to have only a minor effect on the results.

[50] The tidal junction model is highly simplified. The geometry of the tidal junction model only consists of one junction which connects two seaward channels with a tidal river. For example, the Berau channel network is far more complex. The three main channels are interconnected and the network consists of several junctions. The geometry features sharp bends and large depth and width variations. In addition, density gradients may have a substantial effect on subtidal flow division. Differences in density and the associated salt intrusion can result in substantial alterations of the water surface level gradients and baroclinic pressure gradients need to be taken into account. Therefore, these gradients may have a pronounced effect on the subtidal flow division. Extending the theory presented herein to real-world tidal networks is further hampered because deltas often have a dendritic shape, with the length of the branches becoming smaller closer to the coast [*Edmonds and Slingerland*, 2007] and the occurrence of many kinds of dissimilarities in the angles between channels that are connected by a junction.

Table 4. Two Model Configurations That Were Used to Validate Stokes Fluxes of These Models With Observed Fluxes at the Tidal Junction in the Berau Channel Network

	h_1 (m)	h_2 (m)	L_1 (km)	L_2 (km)
Model configuration 1	7	5	60	50
Model configuration 2	10	5	70	50

Table 5. Modeled and Measured Stokes Flux Divided by Width (m^2 s^{-1}) at the Tidal Junction in the Berau Channel Network During Spring and Neap Tide

	Neap Tide		Spring Tide	
	Channel 1	Channel 2	Channel 1	Channel 2
Model configuration 1	−0.07	−0.03	−0.26	−0.12
Model configuration 2	−0.11	−0.02	−0.48	−0.09
Data	−0.10	−0.06	−0.42	−0.28

[51] The tidal junction model presented herein represents a virtual prototype situation with realistic parameter settings. Although the representation of the Berau channel network is highly simplified, an attempt can be made to validate the model by comparing measured and modeled Stokes fluxes. Because there are three main branches in the Berau channel network, we used two different configurations for such a comparison. In configuration 1, parameters are chosen which are representative for the northern and middle branch, whereas in configuration 2 we take parameter values which are representative for the northern and southern channel (Table 4).

[52] Table 5 summarizes the modeled and measured Stokes fluxes per unit width (equation (5)). In channel 1, the observed Stokes flux is in between the two modeled configurations. In channel 2, Stokes fluxes are 2–3 times higher in the observations, which may partly be explained by depth variation in the northern branch of the Berau network. In fact, the depth in the northern channel gradually increases from 5 m at 30 km from the junction to 10 m at 50 km from the junction. In the model the whole 50 km of channel 2 has a depth of 5 m, which damps tides more and causes larger phase differences between flow and water level variation than in the Berau network. The agreement between simulation results and observations is generally good, suggesting that the tidal junction model simulates at least the tidal effect well. Considering that widths of channel 1 and 2 close to the tidal junction are 700 m, these results show that during spring tide the Stokes fluxes in channels 1 and 2 can be similar as the river discharge (Table 5). Further validation of the model is hampered especially by the limited time span of the field surveys. This calls for future hydrographic surveys that cover a full day, which would allow to differentiate between contributions by diurnal tides and the subtidal flow.

[53] The results about the effect of tides on subtidal flow division can also be used to speculate about the implications for sediment division at the apex junction and the morphology of the northern and middle branches in the Berau network. The northern channel in the Berau network is relatively short and shallow. Assuming that hydraulic roughness is equal in the channel network and that sediment divides as the river discharge, the effect of the tidal motion on sediment division is not immediately clear. Tides enhance the allocation of river discharge to the northern branch that is about 10 km shorter and to the middle branch that is 2 m deeper. Because the effect of these depth differences is largest, tides seem to enhance sediment transport into the middle branch of the Berau channel network.

[54] Most riverine sediment is transported seaward during peak river discharges [*Douglas et al.*, 1999]. In comparison with an average river discharge, the division of sediment is more equal, because the high river discharge attenuates the tidal motion. During peak river discharges sediment loads are high and part of the sediments tend to settle in tidal channels. Since the forest area in the Berau river catchment has decreased over the past decades, extreme river discharges are likely to have increased. These three factors may explain that the northern branch has become relatively shallow. It has been receiving a larger share of the alluvial sediments during the past decades than in earlier times.

6. Conclusion

[55] The Berau delta constitutes a network of shallow channels where river flow interacts with the tidal motion. Observations taken at the delta apex junction during spring tide and neap tide indicate that the tidally averaged division of river discharge over the distributaries in the delta may depend on tidal amplitude. Based on this finding, we developed an idealized model of a river branch that splits in two branches that debouch in the sea. The model solves the shallow water equations numerically. At the model boundaries of the sea-connected channels the same tidal forcing is imposed and at the land boundary the model is forced with a constant river discharge. The river discharge splits over the two sea-connected channels as a function of differences in their depth, length or bed roughness (Figure 15).

[56] If one of the sea-connected channels is deeper than the other, the tide enhances the inequality in the subtidal flow division that occurs in the absence of tidal motion. The primary reason is that the deeper channel has smaller relative hydraulic roughness. The magnitude of the tidally induced return discharges that compensate for Stokes fluxes is larger than the magnitude of the Stokes flux, resulting in a net discharge seaward in the deeper channel.

[57] For length differences the tidal motion also enhances the inequality in the division of river discharge generally. Forcing the model only with river discharge, the shorter channel receives more river discharge than the longer one. Tidal energy from the shorter channel partly propagates into the longer channel at the tidal junction, increasing tidal amplitudes in a part of the longer channel close to the junction. The tides steer the river discharge toward the shorter channel, because of the larger subtidal water level gradient and smaller tidal amplitudes in that channel near the junction.

[58] In contrast to differences in depth and length between the sea-connected channels, bed roughness differences result in opposing effects of the tidal motion and of the river discharge on subtidal discharge division. In the absence of tidal motion the channel with the lowest bed roughness receives the highest share of river discharge, whereas tidal motion induces a net discharge from the channel with low bed roughness to the channel with higher bed roughness. The tidally induced residual circulation can be explained from the larger Stokes flux in the channel with smoother bottom, where the tidal range is highest and phase difference between flow velocity and water surface level remains small.

Notation

d Depth from bottom to water surface level (m).
h Vertical distance from bottom to mean sea surface level (m).

ζ Vertical water surface level fluctuation from mean sea level due to tides (m).
s Coordinate along channel, positive seaward (m).
L Length along the s coordinate from river inflow (m).
L_w e-folding length for channel width (m).
W Channel width (m).
Q Total discharge through cross sectional area ($m^3\ s^{-1}$).
Q_S Stokes induced mass flux due to covariation of flow velocity and water level variation ($m^3\ s^{-1}$).
Q_N Net return discharge, compensating for Q_S ($m^3\ s^{-1}$).
U Cross sectional averaged velocity ($m\ s^{-1}$).
g Gravitational acceleration ($m\ s^{-2}$).
C Chézy coefficient ($m^{1/2}\ s^{-1}$).
c_f Bed friction coefficient ($=g/C^2$).
Ψ Discharge asymmetry index $\left(=\frac{\langle Q\rangle_1-\langle Q\rangle_2}{\langle Q\rangle_1+\langle Q\rangle_2}\right)$.
$\langle X\rangle$ tidally averaged X.
X_r a contribution to X due to river discharge only.
X_t a contribution to X due to tidal flow only.
X_i a contribution to X due to interaction of river and tidal flow.
X_{rt} X as a result of forcing with river and tidal flow.
X_1 X in channel 1.
X_2 X in channel 2.

[59] **Acknowledgments.** This study was supported by grant WT 77-203 of WOTRO Science for Global Development, a division of the Netherlands Organisation of Scientific Research (NWO). We acknowledge M.C.G. van Maarseveen (Utrecht University) for preparing and maintaining the instruments and his technical assistance. We thank A. Tarya and E. Wielsma (Utrecht University) for their help during the 2007 field campaign. We are grateful for receiving a MATLAB grid generation program and comments from M. G. Kleinhans (Utrecht University). We also thank C. Huisman and five anonymous reviewers for comments on previous versions of this manuscript.

References

Boiten, W. (2000), *Hydrometry*, A. A. Balkema, Rotterdam, Netherlands.

Bolla Pittaluga, M., R. Repetto, and M. Tubino (2003), Channel bifurcation in braided rivers: Equilibrium configurations and stability, *Water Resour. Res.*, *39*(3), 1046, doi:10.1029/2001WR001112.

Buijsman, M. C., and H. Ridderinkhof (2007), Water transport at subtidal frequencies in the Marsdiep inlet, *J. Sea Res.*, *58*, 255–268, doi:10.1016/j.seares.2007.04.002.

Buschman, F. A., A. J. F. Hoitink, M. van der Vegt, and P. Hoekstra (2009), Subtidal water level variation controlled by river flow and tides, *Water Resour. Res.*, *45*, W10420, doi:10.1029/2009WR008167.

Douglas, I., K. Bidin, G. Balamurungan, N. A. Chappell, R. P. D. Walsh, T. Greer, and W. Sinun (1999), The role of extreme events in the impacts of selective tropical forestry on erosion during harvesting and recovery phases at Danum Valley, Sabah, *Philos. Trans. R. Soc. London, Ser. B*, *354*, 1749–1761.

Edmonds, D. A., and R. L. Slingerland (2007), Mechanics of river mouth bar formation: Implications for the morphodynamics of delta distributary networks, *J. Geophys. Res.*, *112*, F02034, doi:10.1029/2006JF000574.

Edmonds, D. A., and R. L. Slingerland (2008), Stability of delta distributary networks and their bifurcations, *Water Resour. Res.*, *44*, W09426, doi:10.1029/2008WR006992.

Emery, W. J., and R. E. Thomson (2001), *Data Analysis Methods in Physical Oceanography*, 2nd ed., 638 pp., Elsevier, Amsterdam.

Fagherazzi, S., M. Hannion, and P. D'Odorico (2008), Geomorphic structure of tidal hydrodynamics in salt marsh creeks, *Water Resour. Res.*, *44*, W02419, doi:10.1029/2007WR006289.

Friedrichs, C. T., and D. G. Aubrey (1988), Non-linear tidal distortion in shallow well-mixed estuaries: A synthesis, *Estuarine Coastal Shelf Sci.*, *27*, 521–545.

Friedrichs, C. T., and D. G. Aubrey (1994), Tidal propagation in strongly convergent estuaries, *J. Geophys. Res.*, *99*(C2), 3321–3336.

Godin, G. (1991), Frictional effects in river tides, in *Tidal Hydrodynamics*, chap. 19, pp. 379–402, John Wiley, New York.

Godin, G., and A. Martínez (1994), Numerical experiments to investigate the effects of quadratic friction on the propagation of tides in a channel, *Cont. Shelf Res.*, *14*(7–8), 723–748.

Hanert, E., D. Y. Le Roux, V. Legat, and E. Deleersnijder (2005), An efficient Eulerian finite element method for the shallow water equations, *Ocean Modell.*, *10*, 115–136, doi:10.1016/j.ocemod.2004.06.006.

Hill, A. E., and A. J. Souza (2006), Tidal dynamics in channels: Complex channel networks, *J. Geophys. Res.*, *111*, C11021, doi:10.1029/2006JC003670.

Horrevoets, A. C., H. H. G. Savenije, J. N. Schuurman, and S. Graas (2004), The influence of river discharge on tidal damping in alluvial estuaries, *J. Hydrol.*, *294*, 213–228, doi:10.1016/j.jhydrol.2004.02.012.

Jay, D. A. (1991), Green's law revisited: Tidal long-wave propagation in channels with strong topography, *J. Geophys. Res.*, *96*(C11), 20,585–20,598.

Kleinhans, M. G., H. R. A. Jagers, E. Mosselman, and C. Sloff (2008), Bifurcation dynamics and avulsion duration in meandering rivers by one-dimensional and three-dimensional models, *Water Resour. Res.*, *44*, W08454, doi:10.1029/2007WR005912.

Kukulka, T., and D. A. Jay (2003), Impacts of Columbia River discharge on salmonid habitat: 1. A nonstationary fluvial tide model, *J. Geophys. Res.*, *108*(C9), 3293, doi:10.1029/2002JC001382.

Lesser, G. R., J. A. Roelvink, J. A. T. M. van Kester, and G. S. Stelling (2004), Development and validation of a three-dimensional morphological model, *Coastal Eng.*, *51*, 883–915, doi:10.1016/j.coastaleng.2004.07.014.

Muste, M., K. Yu, and M. Spasojevic (2004), Practical aspects of ADCP data use for quantification of mean river flow characteristics; part 1: Moving-vessel measurements, *Flow Meas. Instrum.*, *15*, 1–16, doi:10.1016/j.flowmeasinst.2003.09.001.

Parker, B. B. (1991), The relative importance of the various nonlinear mechanisms in a wide range of tidal interactions (review), in *Tidal Hydrodynamics*, chap. 13, pp. 237–268, John Wiley, New York.

Ramamurthy, A. S., J. Qu, and D. Vo (2007), Numerical and experimental study of dividing open-channel flow, *J. Hydraul. Eng. Am. Soc. Civ. Eng.*, *133*(10), 1135–1144, doi:10.1061/(ASCE)0733-9429(2007)133:10(1135).

Ridderinkhof, H. (1988), Tidal and residual flows in the western Dutch Wadden Sea I: Numerical model results, *Neth. J. Sea Res.*, *22*(1), 1–21.

Schlax, M. G., and D. B. Chelton (1992), Frequency domain diagnostics for linear smoothers, *J. Am. Stat. Assoc.*, *87*(420), 1070–1081.

Stein, U., and P. Alpert (1993), Factor separation in numerical simulations, *J. Atmos. Sci.*, *50*(14), 2107–2115.

Wang, Z. B., R. J. Fokkink, M. de Vries, and A. Langerak (1995), Stability of river bifurcations in 1D morphodynamic models, *J. Hydraul. Res.*, *33*(6), 739–750.

Warner, J. C., D. Schoellhamer, and G. Schladow (2003), Tidal truncation and barotropic convergence in a channel network tidally driven from opposing entrances, *Estuarine Coastal Shelf Sci.*, *56*, 629–639, doi:10.1016/S0272-7714(02)00213-5.

F. A. Buschman, P. Hoekstra, and M. van der Vegt, Institute for Marine and Atmospheric Research Utrecht, Department of Physical Geography, Faculty of Geosciences, Utrecht University, PO Box 80.115, NL-3508 TC Utrecht, Netherlands. (f.buschman@geo.uu.nl; p.hoekstra@geo.uu.nl; m.vandervegt@geo.uu.nl)

A. J. F. Hoitink, Hydrology and Quantitative Water Management Group, Department of Environmental Sciences, Wageningen University, PO Box 47, NL-6700 AA Wageningen, Netherlands. (ton.hoitink@wur.nl)